Synthesis and Characterization of Porous Magnesium Hydroxide and Oxide Nanoplates

Jimmy C. Yu,*,[†] **Anwu Xu,**[†] **Lizhi Zhang,**[†] **Ruiqi Song,**[‡] **and Ling Wu**[†]

Department of Chemistry, The Chinese University of Hong Kong, Shatin, New Territories, Hong Kong, China, and School of Chemistry and Chemical Engineering, Zhongshan University, Guangzhou 510275, China

Received: May 15, 2003; In Final Form: October 24, 2003

Porous magnesium hydroxide nanoplates were prepared directly from commercial bulk magnesium oxide crystals by a simple hydrothermal treatment. These thin plates would aggregate into large spherical particles. The platelike morphology was retained after calcination, and porous magnesium oxide nanoplates were obtained. These plates have a wormhole-like porous structure with high surface area. The obtained materials exhibit bimodal pore size distributions in the mesoporous domain. The aggregation of the nanoplates gives rise to large mesopores with a size of about 36 nm. In addition, each plate has small wormhole mesopores with a size of about 3.7 nm. The growth of magnesium hydroxide nanoplates occurred through a dissolution−recrystallization process. X-ray diffraction and electron diffraction, transmission electron microscopy, scanning electron microscopy, and nitrogen sorption have been employed to characterize these nanoplates. Such porous nanoplates with high surface area and high crystallinity have many promising applications. Moreover, bismuth oxide nanoplates were also produced following a similar method. The formation mechanism of such mesostructures without the use of a template is also discussed.

Introduction

Magnesium hydroxide (brucite) is commonly used as the flame-retardant filler in composite materials due to its ability to undergo endothermic dehydration in fire conditions,[1−3] as well as a precursor for the preparation of magnesium oxide.[4] Magnesium oxide (MgO, periclase) is a homomorphous compound with rocksalt structure. Its ionic constituents consist of a relatively small number of electrons and have stable oxidation states. Due to these properties, it is likely that MgO exhibits a limited number of reasonably well-defined surface defect structures such as low coordinated ions and/or vacancies on the surface. In recent years, MgO has become one of the preferred targets of surface structural analysis and catalytic research.[5−7] It has been reported that nanocrystalline MgO exhibits voracious adsorbent properties due to both enhanced surface areas and intrinsically higher surface reactivities.[8,9] MgO has been widely used in catalysis, toxic waste remediation, or as additives in refractory, paint, and superconductor products, and is also used in steel manufacturing because it is highly corrosion-resistant.[10] In addition, MgO is a typical wide band gap insulator, and its electronic and optical properties have been investigated.[11−13] A number of methods have been developed for the preparation of porous MgO materials.[2,8] However, there has been no report on the large-scale synthesis of pure porous $Mg(OH)_2$ and MgO with nanoplate morphology directly from the commercial bulk MgO crystals.

The synthesis of mesoporous materials represents a significant benchmark in modern materials chemistry. Mesoporous materials are often synthesized via a surfactant-templating formation process.[14] Wormhole mesoporous materials are generally more active heterogeneous catalysts in comparison to their ordered hexagonal analogues. The enhanced reactivity has been at-tributed, in part, to a mesopore framework that is connected in three dimensions, allowing the guest molecules to more readily access reactive centers that have been designed into the framework surfaces.[15] Therefore, considerable attention has been focused on wormhole porous materials due to their potential technological applications.[14,16] Moreover, the synthesis of porous materials with controlled morphology, size, chemical composition, and crystal structure is of great importance in industry.[17] Although attempts have been made, the control of shape is still a challenge.[18,19]

Recently, we have obtained rare earth hydroxide nanotubes directly from the corresponding bulky crystals by a hydrothermal recrystallization process.[20] Here, we extend this method to synthesize porous $Mg(OH)_2$ crystalline nanoplates using commercial bulk MgO as the starting material in the absence of any surfactants. Porous MgO nanoplates were then obtained through calcination of the as-synthesized $Mg(OH)_2$ sample. In comparison with conventional surfactant-templating methods, the new approach is simple and more suitable for industrial-scale production. Since surfactants are not required in the synthesis, products of very high purity can be obtained. Moreover, α-Bi_2O_3 nanocrystals with uniform platelike morphology and narrow size distributions can also be produced by a similar method.

Experimental Section

Preparation. Our synthesis is based on hydrothermal treatment of commercial bulk MgO crystals under certain conditions. Porous $Mg(OH)_2$ nanoplates were prepared as follows. In a typical synthesis, 0.4 g of MgO powders (Aldrich, 99.9% purity) was added in 16 mL of water, then poured into a stainless Teflon-lined 20 mL capacity autoclave. The autoclave was sealed and maintained at 160 °C for 24 h, and then air cooled to room temperature. The resulting product was collected and washed with water and dried at 80 °C in air for further characterization. The obtained $Mg(OH)_2$ product was calcined

---
* Address correspondence to this author. Fax: 852 2603 5057. E-mail: jimmyu@cuhk.edu.hk.
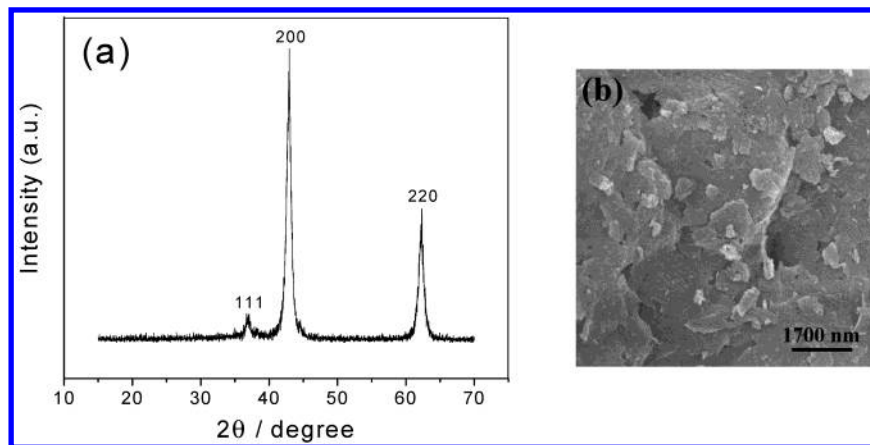[†] The Chinese University of Hong Kong.
[‡] Zhongshan University.

Magnesium Hydroxide and Oxide Nanoplates

J. Phys. Chem. B, Vol. 108, No. 1, 2004 **65**

Figure 1. XRD pattern (a) and SEM image (b) of the raw material (bulk MgO crystals).

to produce MgO at 450 °C for 4 h in air. Bismuth oxide product was directly obtained by hydrothermal treatment, using the commercial bismuth oxide as the starting material.

Characterization. The low-angle and wide-angle X-ray powder diffraction (XRD) patterns of all samples were per-formed on a Brucker D8-advance X-ray diffractometer with Cu Kα radiation ($\lambda = 1.5418$ Å), with the operation voltage and current maintained at 40 kV and 40 mA, respectively. Scanning electron microscopic (SEM) images were obtained with a JEOL JSM-6330F operated at a beam energy of 20.0 kV. Transmission electron microscopic (TEM) images, high-resolution transmis-sion electron microscopic (HRTEM) images, and selected area electron diffraction (SAED) patterns were obtained on a JEOL-2010 microscope with an accelerating voltage of 200 kV. Sample grids were prepared by sonicating powdered samples in ethanol for 20 min and evaporating one drop of the suspension onto a carbon-coated, holey film supported on a copper grid for TEM measurements. Thermogravimetric analysis was carried out under a stream of nitrogen, at a heating rate of 5 °C/min, using a Netzsch TGA-209. Differential scanning calorimetric (DSC) analysis of the sample in a crimped aluminum crucible was carried out up to a temperature of 500 °C, using a Netzsch DSC-204 under a stream of nitrogen, at a heating rate of 5 °C/min. Nitrogen adsorption measurements were performed at 77 K, using a Micromeritics ASAP 2010 system utilizing Barrett−Emmett−Teller (BET) calculations for surface area and BJH calculations for pore size distribution for the desorption branch of the isotherm.

Results and Discussion

The X-ray diffraction (XRD) pattern and the scanning electron microscopy (SEM) image of the starting MgO crystals are shown in Figure 1, panels a and b, respectively. The raw material is bulk MgO polycrystalline and has irregularly shaped large particles (Figure 1b). $Mg(OH)_2$ nanoplates can be easily obtained under hydrothermal treatment of the MgO crystals at 160 °C for 24 h. The wide-angle XRD pattern of the obtained $Mg(OH)_2$ nanoplates is shown in Figure 2a. All diffraction peaks of the XRD pattern in Figure 2 can be perfectly indexed to a pure hexagonal phase [space group $P3m1$ (164)] of $Mg(OH)_2$ with calculated lattice constants $a = 3.15$ Å and $c = 4.78$ Å, in agreement with the reported data (JCPDS 7-239). The crystalline phase of the resulting products is different from that of the starting material (Figures 1a and 2). The low angle for the obtained $Mg(OH)_2$ product contains a broad diffraction peak centered at 7.6 nm (Figure 2b), indicating the product has a wormlike mesoporous structure.
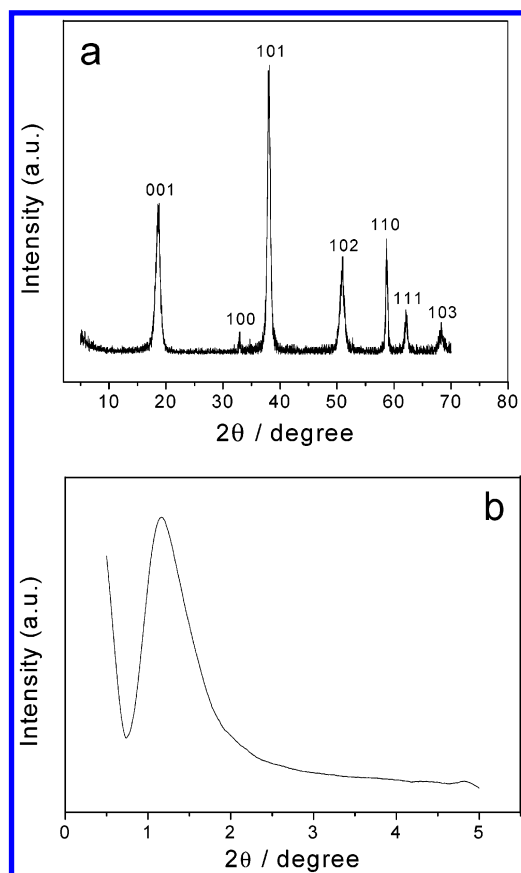

Figure 2. Wide-angle (a) and low-angle (b) XRD patterns of the as-synthesized $Mg(OH)_2$ nanoplates by the hydrothermal method at 160 °C.

The morphology of the $Mg(OH)_2$ product was visualized by SEM measurements. As shown in Figure 3a, the sample has a spherical morphology. A higher magnification SEM image (Figure 3b) taken from the white box in Figure 3a reveals that each spherical $Mg(OH)_2$ particle consists almost entirely of well-defined hexagonal nanoplates with a thickness of 50−110 nm and lateral dimensions of several micrometers, which is of very different morphology than the starting material (Figure 1b). The overall hexagonal morphology of these platelike particles is consistent with the hexagonal crystallographic characteristics of brucite. It is clearly shown that the $Mg(OH)_2$ nanoplates aggregate into large spherical particles with the diameter of several tens of micrometers. The results demonstrate that $Mg(OH)_2$ nanoplates in high yields (∼100%) can be obtained by this simple method.
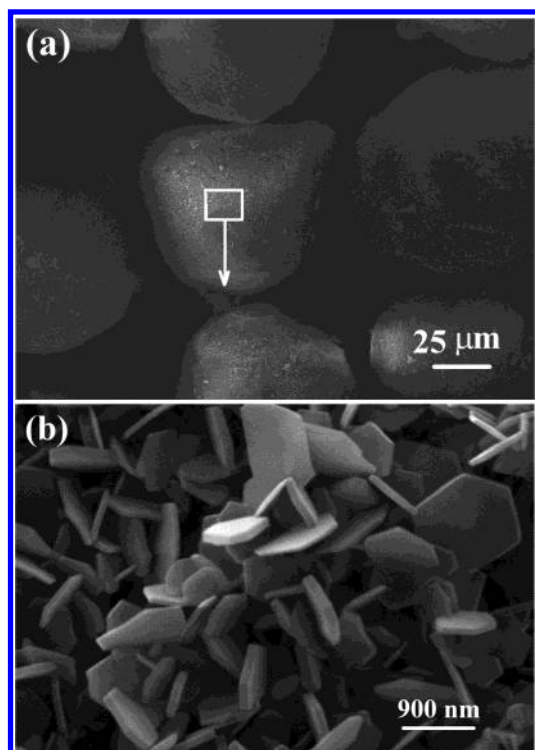
Figure 3. (a) Low-magnification SEM image of the obtained Mg-(OH)$_2$ shows spherical morphology. (b) Higher magnification SEM image of the product shows a hexagonal platelike nanostructure.

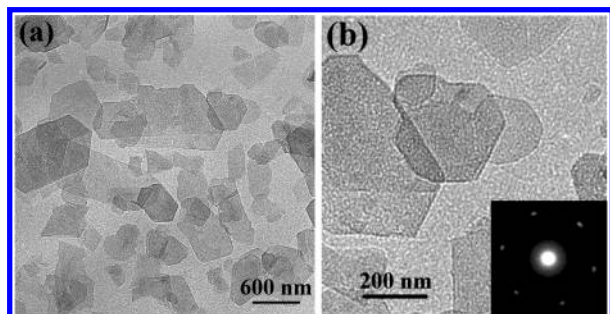**Figure 4.** (a) A typical TEM image of the obtained porous Mg(OH)$_2$ nanoplates at a low magnification. (b) TEM image of the porous Mg-(OH)$_2$ nanoplates at a higher magnification. Inset: A selected area electron diffraction pattern of a single nanoplate.

Figure 5. A typical HRTEM image of a single Mg(OH)$_2$ nanoplate clearly showing the presence of mesopores (arrows point to pores).

Figure 6. Schematic illustration of the formation of wormhole-like mesoporous Mg(OH)$_2$ nanoplates from bulk MgO particles under hydrothermal treatment.

The morphology and structure of the Mg(OH)$_2$ product were further examined with transmission electron microscopy (TEM) and selected area electron diffraction (SAED). Figure 4a shows the low-magnification TEM image of the obtained Mg(OH)$_2$ nanoplates. Imaging at higher magnification shows the presence of wormlike mesopores with a pore size of about 3.8 nm. A SAED pattern (inset) taken from a single nanoplate (Figure 4b) can be indexed as a hexagonal Mg(OH)$_2$ crystal structure. Figure 5 shows a typical HRTEM image of a single nanoplate. Lattice fringes showing the nature of highly crystalline Mg(OH)$_2$ and mesopores (black arrows are pointing to these regions) on the nanoplate are clearly observed in Figure 5.

It should be noted that such mesoporous structure is obtained without the use of structure-directing reagents such as surfactants. This can avoid the surfactant removal step, which causes the collapse of the mesoporous structure. The formation of such mesopores can be illustrated in Figure 6. First, bulk MgO crystals are dissolved in water and hydroxylated into Mg(OH)$_2$ primary particles. These particles are then aggregated to produce large platelike particles through oriented attachment. Banfield et al. provided strong evidence that some natural
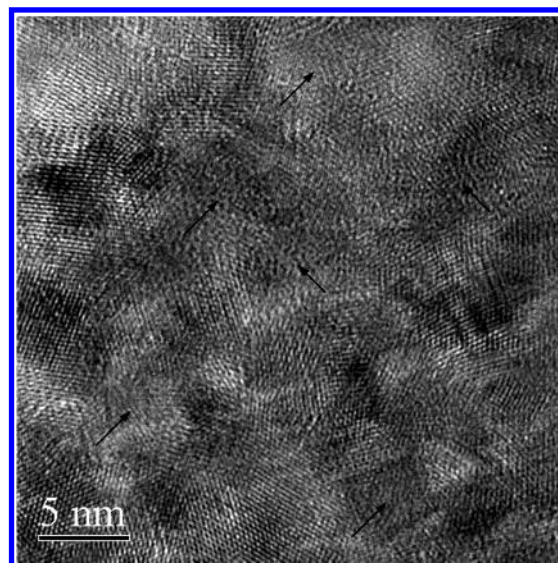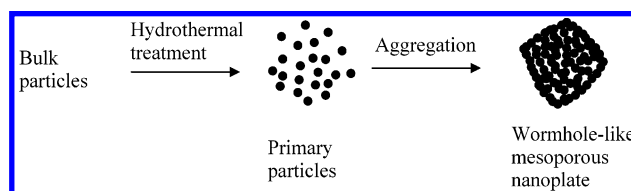
minerals and synthetic nanocrystals could grow through a mechanism of oriented attachment of nanocrystals.[21] Finally, wormhole-like mesoporous Mg(OH)$_2$ nanoplates are formed under hydrothermal treatment, and the interagglomeration of the nanoplates gives rise to textural mesopores with a size of about 36 nm.

When the Mg(OH)$_2$ nanoplates were calcined at 450 °C in air for 4 h, MgO nanoplates were obtained. Figure 7a shows a typical wide-angle XRD pattern of the obtained MgO product. All of the peaks in Figure 7 can be readily indexed to a pure face-centered cubic phase [space group *Fm3m* (225)] of transformed MgO with calculated lattice constants $a = 4.21$ Å (JCPDS 87-0653). The low-angle XRD pattern shown in Figure 7b clearly presents a broad peak centered at 7.2 nm, indicating a wormlike mesoporosity. The basal spacing decreases from 7.6 nm to 7.2 nm as Mg(OH)$_2$ is converted to MgO by calcination.

A typical SEM image of the obtained MgO product clearly shows that the platelike feature is fully retained in the final MgO sample after calcination (Figure 8). Moreover, the large spherical morphology is also maintained. This fact suggests that a morphological preservation might be achieved during the structure rearrangement process of a hexagonal ABAB... structure into a cubic ABCABC... structure. The size of MgO nanoplates is smaller to that of Mg(OH)$_2$ because the former has a higher density.

A representative TEM image of the MgO nanoplates at a lower magnification is shown in Figure 9a. A higher magnification TEM image of the obtained MgO nanoplates shows that the plates have wormlike mesoporosity and the pore size measured from the TEM image is about 3.7 nm (Figure 9b). The composition of the nanoplates as extracted from the energy-dispersive X-ray spectroscopy (EDX) analysis gives a Mg:O

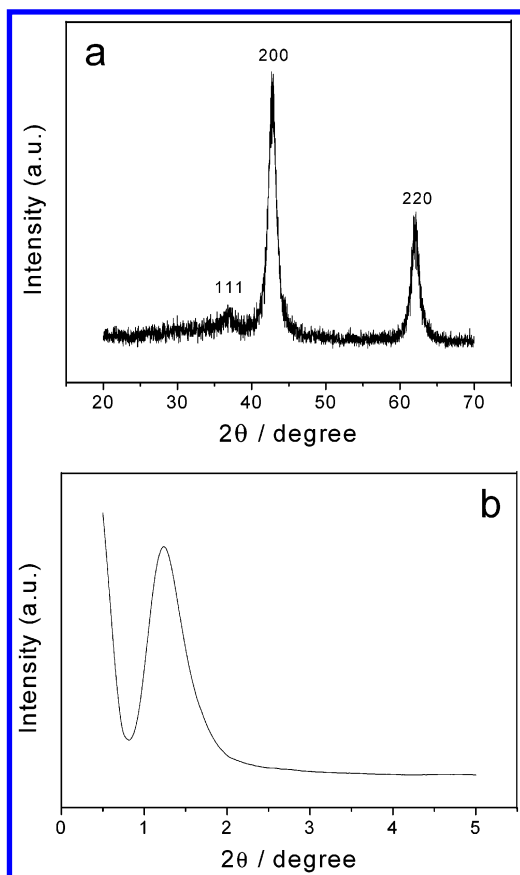Magnesium Hydroxide and Oxide Nanoplates

J. Phys. Chem. B, Vol. 108, No. 1, 2004 **67**

Figure 7. Wide-angle (a) and low-angle (b) XRD patterns of the porous MgO nanoplates produced from Mg(OH)$_2$ nanoplates by calcination at 450 °C for 4 h.
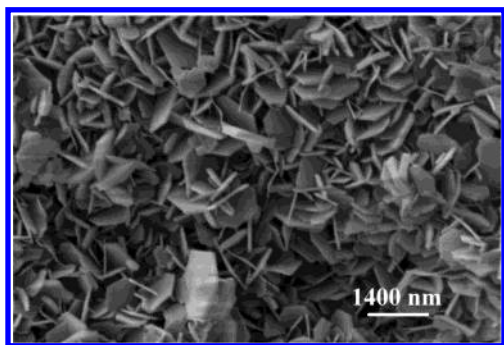

Figure 8. SEM image of porous MgO nanoplates obtained by calcination of Mg(OH)$_2$ nanoplates at 450 °C.
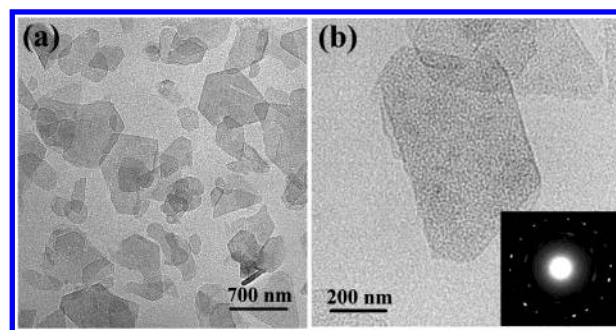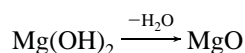

Figure 9. (a) Low-magnification TEM image of the obtained MgO nanoplates. (b) TEM image of the porous MgO nanoplates at a higher magnification. Inset: A selected area electron diffraction pattern of a single nanoplate.
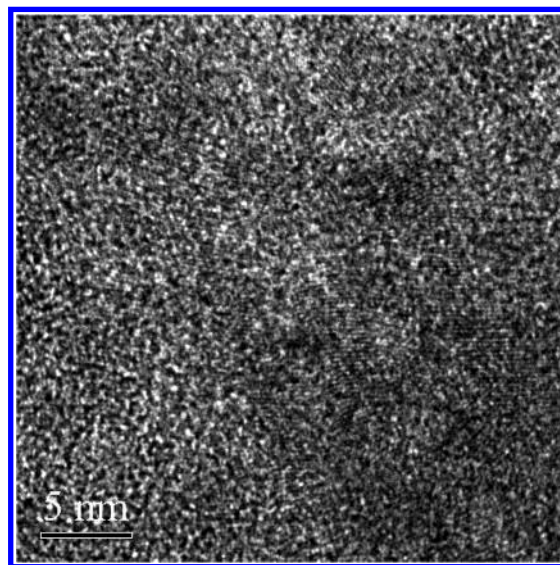

Figure 10. A typical HRTEM image of a single MgO nanoplate showing wormhole-like mesopores on the plate and lattice fringes for crystalline MgO.
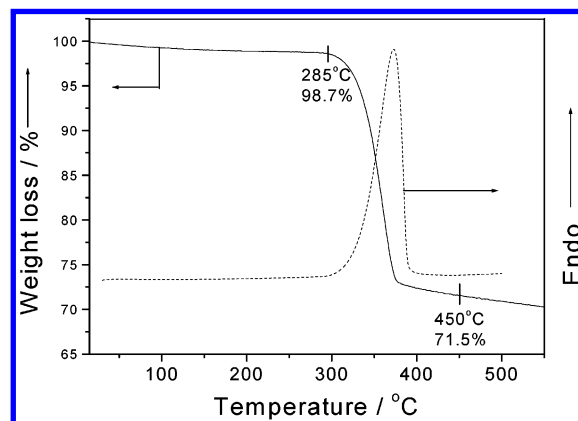

Figure 11. Thermogravimetric trace (solid line) and differential scanning calorimetric (DSC) plot (dashed line) of the as-synthesized porous Mg(OH)$_2$ products.

atomic ratio of 1:1 in the calcined sample. The nanoplates are therefore confirmed to be MgO crystals. The electron diffraction pattern (Figure 9b, inset) clearly demonstrates a cubic structure for the (200) and (220) planes of MgO, and the diffraction rings reveal that it has polycrystalline features. Figure 10 shows an HRTEM image of MgO nanoplates. Lattice fringe for MgO and wormhole-like mesopores can be clearly seen from this image.

The TGA and DSC measurements were carried out to analyze the thermal behavior and decomposition process of the obtained Mg(OH)$_2$ products. A representative TGA-DSC profile is shown in Figure 11. A pronounced weight loss step is found in the temperature range of 280−450 °C, and a corresponding well-defined endothermic peak is observed near 358 °C. This can be ascribed to the decomposition of Mg(OH)$_2$:

$$Mg(OH)_2 \xrightarrow{-H_2O} MgO$$

However, the theoretical weight loss for the Mg(OH)$_2 \rightarrow$ MgO transformation is 30.8%, which is slightly higher than the observed 28.5%. We ascribe it to the incompleteness of the decomposition reaction in this temperature range. This result is in agreement with the previous reports.[22,23]

Representative nitrogen desorption/adsorption isotherms and the corresponding BJH (Barret−Joyner−Halenda) pore size distribution curve (inset) of the obtained Mg(OH)$_2$ product are shown in Figure 12. The N$_2$ isotherm of the as-synthesized Mg-
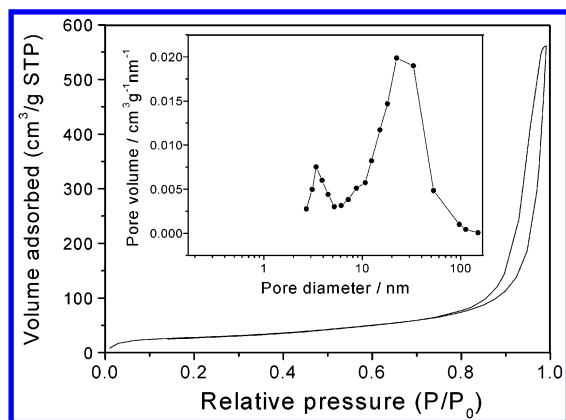
Figure 12. Nitrogen adsorption−desorption isotherms for the obtained porous $Mg(OH)_2$ product for 6 h. Inset: Corresponding Barret−Joyner−Halenda (BJH) pore size distribution curve determined from the N_2 desorption isotherm. Prior to measurement the sample was evacuated at 523 K and 10^{-6} Torr for 16 h.

Figure 13. Nitrogen adsorption−desorption isotherms for the obtained porous MgO nanoplates for 6 h. Inset: Corresponding Barret−Joyner−Halenda (BJH) pore size distribution curve determined from the N_2 desorption isotherm. Prior to measurement the sample was evacuated at 523 K and 10^{-6} Torr for 16 h.
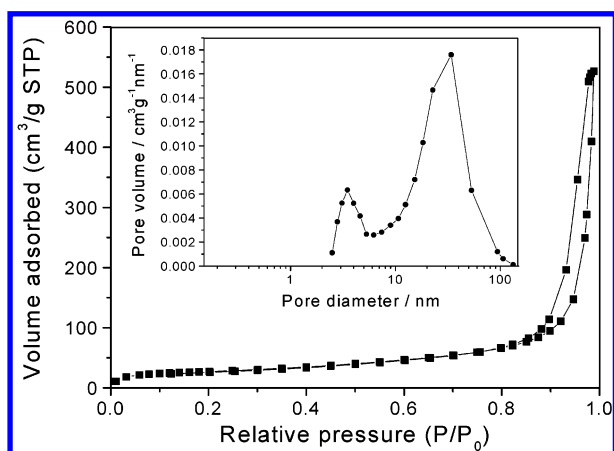
$(OH)_2$ is a type III isotherm with a large type H_3 hysteresis loop.[24] The type H3 loop, which does not exhibit any limiting adsorption at high $P/P°$, is observed with aggregates of platelike particles giving rise to slit-shaped pores. The synthesized porous $Mg(OH)_2$ product has a high BET surface area of 100 m^2 g^{-1}. The pore size distribution, as calculated by the BJH method from the desorption branch of the nitrogen isotherm, reveals that this material contains small mesopores with a pore size of 3.6 nm and large mesopores with a pore size of 36 nm. The former mesopores exist among small primary nanoparticles in the nanoplates, which is in agreement with TEM observations. The latter textural mesopores are formed by the aggregation of the thin nanoplates (inset in Figure 12). This textural charac-teristics differentiate our porous $Mg(OH)_2$ products from conventionally prepared nonporous $Mg(OH)_2$.

Figure 13 shows representative nitrogen adsorption/desorption isotherms and the corresponding BJH pore size distribution curve (inset) of the obtained MgO product. The N_2 isotherm of the MgO product is also a type III isotherm with a large type H_3 hysteresis loop, indicating MgO has large textural mesopores arising from aggregates of platelike particles.[2c] The obtained MgO product has a high BET surface area of 97 m^2 g^{-1}. The BJH analyses show that it also exhibits bimodal mesopore distribution with sizes of 3.5 and 35 nm (inset in Figure 13). The pore size of the small mesopores in each plate is consistent
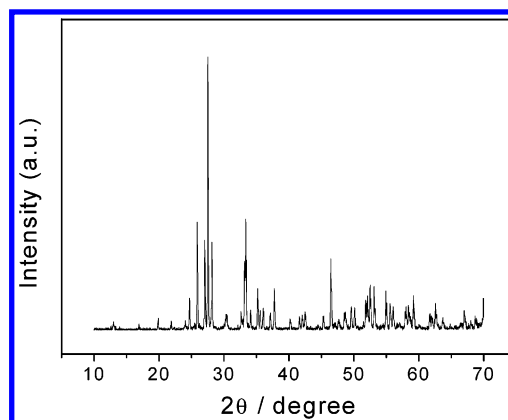

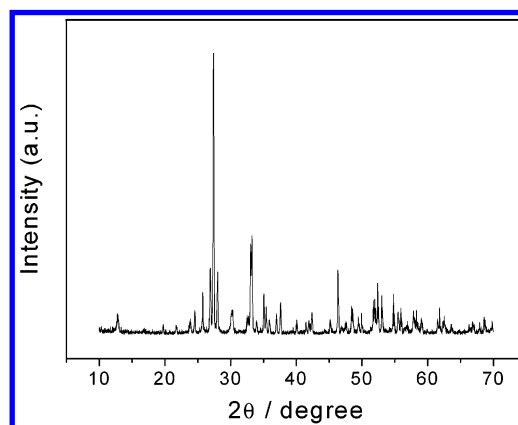**Figure 14.** XRD pattern of the commercial α-Bi_2O_3 raw material.

Figure 15. XRD pattern of α-Bi_2O_3 nanoplates obtained by hydro-thermal treatment of commercial bulk Bi_2O_3 crystals at 160 °C for 24 h.

with TEM observations (Figure 9b). It has been proven that such a hierarchical combination of independently controlled, well-connected smaller and larger mesopores could reduce transport limitations in catalysis, resulting in higher activities and better controlled selectivities.[25] These bimodal mesoporous $Mg(OH)_2$ and MgO materials may find promising applications in catalysis since their larger abundant textural mesopores can provide reactant substances of different size transport circum-stance comparable to those in open medium.[26]

This novel method can be extended to synthesize other materials with platelike nanostructure. By using commercial α-Bi_2O_3 as the precursor (Figure 14), α-Bi_2O_3 nanoplates can also be produced by a hydrothermal recrystallization process. The XRD pattern of the obtained α-Bi_2O_3 products under hydrothermal treatment of the commercial bulk α-Bi_2O_3 crystals at 160 °C for 24 h is shown in Figure 15. All diffraction peaks match well that reported in the literature (JCPDS Card No 27-54). The crystalline phase of the resulting products is the same as that of the starting material (Figures 14 and 15). A typical SEM image of the as-synthesized α-Bi_2O_3 sample is shown in Figure 16. The product consists of a large number of thin nanoplates with a thickness of 30−90 nm and lateral dimensions of about 1 μm. In contrast to $Mg(OH)_2$ products, no mesopores can be observed on α-Bi_2O_3 plates by TEM measurements (Figure 17). The ED pattern recorded from a single plate shows that each nanoplate is a single crystal (inset in Figure 17). Some metal oxides, such as MgO, rare earth oxides, can be transformed into corresponding hydroxides by hydrothermal treatment.[22] Other metal oxides, such as Bi_2O_3, ZnO, and MnO_2,[27] do not produce corresponding hydroxides during hydrothermal treatment. The main reason is that these
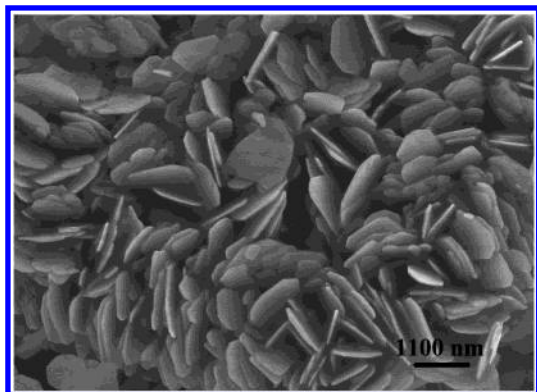
Magnesium Hydroxide and Oxide Nanoplates

J. Phys. Chem. B, Vol. 108, No. 1, 2004 **69**

Figure 16. A typical SEM image of the as-synthesized α-Bi₂O₃ products with platelike morphology.

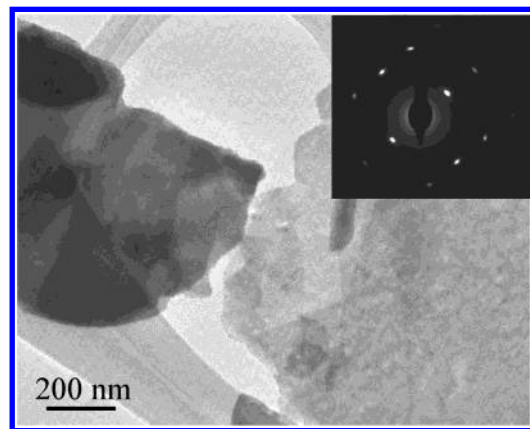**Figure 17.** The TEM image of obtained α-Bi₂O₃. Inset: ED pattern of a single plate.

metal hydroxides such as Bi(OH)₃ are hydrothermally unstable. It has been reported that Bi(OH)₃ would decompose to α-Bi₂O₃ under hydrothermal treatment at 100 °C for 10 h.[28]

Although the exact growth mechanism of magnesium hydroxide and bismuth oxide nanoplates is still unclear at present, our results show that the formation of the nanoplates is probably caused by the dissolution−recrysatllizatoin processes. As the starting material in our synthesis is pure oxide powders, it is most likely that the growth is governed by a solution−solid (SS) process. The oxide molecules are first dissolved from the starting oxide under hydrothermal treatment, and then directly recrystallize and grow into platelike nanostructures through a dissolution−recrystallization mechanism.[29] The crystalline MgO and Bi₂O₃ are generally considered as insoluble in water under normal conditions. However, our experimental results show that under hydrothermal conditions these oxides can be dissolved in water and then recrystallize. This dissolution−recrystallization process is mainly related to changes in the temperature and pressure of the system. When the temperature and pressure of the system increase during hydrothermal treatment, the bulky crystalline MgO gradually dissolves in the water. The dissolved MgO is hydroxylated into the corresponding hydroxide, i.e., Mg(OH)₂. As the concentration of Mg(OH)₂ increases beyond saturation, the hydroxide crystallizes as primary particles. These particles aggregate to form large platelike particles. It is obvious that bulk particles rather than ionic species are the precursors for further nanoplate growth, significantly different from previous reports based on a homogeneous nucleation and solution growth process.[30] We propose a related SS mechanism in which the precursor is delivered in a solution rather than in the vapor phase, an analogy to the vapor−solid (VS) process for nanobelts growth.[31] It is well-known that the most important factor

affecting the growth process of single crystals from a solution is the solubility of the solutes. At high pressure and temperature the solubility of many oxides becomes very appreciable in water or water with a small amount of mineralizer. In our previous study, rare earth hydroxide nanotubes and MnO₂ nanowires were produced by hydrothermal treatment of the corresponding oxides.[20,27] However, in this study, platelike morphology was observed by the same method. We believe this could be related to the inherent crystal structure of these materials. A thorough investigation is under way to generalize the underlying growth principle and thus to exploit it for the synthesis of other nanomaterials with controlled morphologies and sizes. The synthesis of Mg(OH)₂ or α-Bi₂O₃ nanoplates can easily be reproduced and scaled up. By using a large autoclave (500 mL) for the hydrothermal treatment, a production of tens of grams of the samples can be obtained.

Conclusions

The present study shows that crystalline porous Mg(OH)₂ nanoplates can be synthesized from corresponding bulky crystals by a facile hydrothermal recrystallization process. This solid−solution−solid transformation is virtually complete with a yield of ∼100%. The growth of magnesium hydroxide nanoplates is probably caused by a dissolution−recrystallization process. Porous MgO nanoplates may be obtained by a subsequent thermal decomposition of the Mg(OH)₂ samples. The morphological feature of the starting Mg(OH)₂ material is well retained during the thermal treatment process. The crystals of the Mg-(OH)₂ and MgO nanoplates have a wormhole-like structure. They possess high specific surface areas that would make them attractive in the field of catalysis. The formation of bimodal mesopores is believed to be caused by the aggregation of small primary nanoparticles in nanoplates. These plates finally aggregate into larger spherical particles, and hierarchically structured materials at multiple length scales were obtained. α-Bi₂O₃ nanoplates were also prepared by a similar method. These materials may find applications in solid oxide fuel cells, oxygen sensors, and catalysis. The simplicity of the hydrothermal process, low cost, and availability of raw materials would favor scaled-up industrial manufacturing. We think that this novel method may be extended to synthesize other metal hydroxide and oxide nanomaterials with controlled morphology and size directly from the corresponding bulky crystals.

References and Notes

(1) Rothon, R. N. *Magnesium hydroxide: New Products, Processes and Applications*; Intertech: Portland, MA; Functional Effect Filler: Berlin, Germany, 2000.

(2) (a) Henrist, C.; Mathieu, J. P.; Vogels, C.; Rulmont, A.; Cloots, R. *J. Cryst. Growth* **2003**, *249*, 321. (b) Van Aken, P. A.; Langenhorst, F. *Eur. J. Mineral.* **2001**, *13*, 329. (c) Ding, Y.; Zhang, G. T.; Wu, H.; Hai, B.; Wang, L. B.; Qian, Y. T. *Chem. Mater.* **2001**, *13*, 435. (d) Utamapanya, S.; Klabunde, K. J.; Schlup, J. R. *Chem. Mater.* **1991**, *3*, 175.

(3) Durin-France, A.; Ferry, L.; Lopez Cuesta, J. M.; Crespy, A. *Polym. Int.* **2000**, *49*, 1101.

(4) Li, Y. D.; Sui, M.; Ding, Y.; Zhang, G. H.; Zhuang, J.; Wang, C. *Adv. Mater.* **2000**, *12*, 818.

(5) Diwald, O.; Knözinger, E. *J. Phys. Chem. B* **2002**, *106*, 3495.

(6) Anpo, M.; Yamada, Y.; Kubokawa, Y.; Coluccia, S.; Zecchina, A.; Che, M. *J. Chem. Soc., Faraday Trans.* **1988**, *84*, 751.

(7) Murphy, D. M.; Farley, R. D.; Purnell, I. J.; Rowlands, C. C.; Yacob, A. R.; Paganini, M. C.; Giamello, E. *J. Phys. Chem. B* **1999**, *103*, 1944.

(8) Richards, R.; Li, W. F.; Decker, S.; Davidson, C.; Koper, O.; Zaikovski, V.; Volodin, A.; Rieker, T.; Klabunde, K. J. *J. Am. Chem. Soc.* **2000**, *122*, 4921.

(9) Khaleel, A.; Kapoor, P. N.; Klabunde, K. J. *Nanostruct. Mater.* **1999**, *12*, 463.

(10) (a) Richards, R.; Mulukutla, R. S.; Mishakov, I.; Chesnokov, V.; Volodin, A.; Zaikovski, V.; Sun, K. J.; Klabunde, K. J. *Scr. Mater.* **2001**, *44*, 1663. (b) Rajagopalan, S.; Koper, O.; Decker, S.; Klabunde, K. J. *Chem. Eur. J.* **2002**, *8*, 2602. (c) Choudary, B. M.; Mulukutla, R. S.; Klabunde, K. J. *J. Am. Chem. Soc.* **2003**, *125*, 2020.

(11) Sterrer, M.; Berger, T.; Diwald, O.; Knözinger, E. *J. Am. Chem. Soc.* **2003**, *125*, 195.

(12) Rosenblatt, G. H.; Rowe, M. W.; Williams, G. P.; Williams, R. T., Jr.; Chen, Y. *Phys. Rev. B* **1989**, *39*, 10309.

(13) Grant, J. L.; Cooper, R.; Zeglinski, P.; Boas, J. F. *J. Chem. Phys.* **1989**, *90*, 807.

(14) (a) Beck, J. S.; Vartuli, J. C.; Roth, W. J.; Leonowicz, M. E.; Kresge, C. T.; Schmitt, K. D.; Chu, C. T.-W.; Olson, D. H.; Sheppard, E. W.; McCullen, S. B.; Higgins, J. B.; Schlenker, J. L. *J. Am. Chem. Soc.* **1992**, *114*, 10834. (b) Ying, J. Y.; Mehnert, C. P.; Wong, M. S. *Angew. Chem., Int. Ed. Engl.* **1999**, *38*, 56.

(15) (a) Fan, J.; Yu, C.; Wang, L.; Tu, B.; Zhao, D.; Sakamoto, Y.; Terasaki, O. *J. Am. Chem. Soc.* **2001**, *123*, 12113. (b) Kim, S. S.; Pauly, T. R.; Pinnavaia, T. J. *Chem. Commun.* **2000**, 835.

(16) (a) Hu, J. T.; Odom, T. W.; Lieber, C. M. *Acc. Chem. Res.* **1999**, *32*, 435. (b) Duan, X.; Huang, Y.; Cui, Y.; Wang, J.; Lieber, C. M. *Nature* **2001**, *409*, 66. (c) El-Sayed, M. A. *Acc. Chem. Res.* **2001**, *34*, 257.

(17) (a) Maillard, M.; Giorgio, S.; Pileni, M. P. *Adv. Mater.* **2002**, *14*, 1084. (b) Murphy, C. J.; Jana, N. R. *Adv. Mater.* **2002**, *14*, 80. (c) Nelson, J. A.; Wagner, M. J. *J. Am. Chem. Soc.* **2003**, *125*, 332. (d) Kovtyukhova, N. I.; Mallouk, T. E. *Chem. Eur. J.* **2002**, *8*, 4355.

(18) (a) Xia, Y. N.; Yang, P. D.; Sun, Y. G.; Wu, Y. Y.; Mayers, B.; Gates, B.; Yin, Y. D.; Kim, F.; Yan, H. Q. *Adv. Mater.* **2003**, *15*, 353. (b) Yu, S. H.; Yoshimura, M. *Adv. Mater.* **2002**, *14*, 296. (c) Dai, Z. R.; Pan, Z. W.; Wang, Z. L. *J. Am. Chem. Soc.* **2002**, *124*, 8673.

(19) (a) Wirtz, M.; Parker, M.; Kobayashi, Y.; Martin, C. R. *Chem. Eur. J.* **2002**, *8*, 3572. (b) Niederberger, M.; Muhr, H.-J.; Krumeich, F.; Bieri, F.; Günther, D.; Nesper, R. *Chem. Mater.* **2000**, *12*, 1995. (c) Kuang, D. B.; Xu, A. W.; Fang, Y. P.; Ou, H. D.; Liu, H. Q. *J. Cryst. Growth* **2002**, *244*, 379.

(20) (a) Xu, A. W.; Fang, Y. P.; You, L. P.; Liu, H. Q. *J. Am. Chem. Soc.* **2003**, *125*, 1494. (b) Fang, Y. P.; Xu, A. W.; You, L. P.; Song, R. Q.; Yu, J. C.; Zhang, H. X.; Li, Q.; Liu, H. Q. *Adv. Funct. Mater.* **2003**, *13*, 955.

(21) (a) Banfield, J. F.; Welch, S. A.; Zhang, H. Z.; Ebert, T. T.; Penn, R. L. *Science* **2000**, *289*, 751. (b) Penn, R. L.; Banfield, J. F. *Geochim. Cosmochim. Acta* **1999**, *63*, 1549.

(22) Wang, J. A.; Novaro, O.; Bokhimi, X.; López, T.; Gómez, R.; Navarrete, J.; Llanos, M. E.; López-Salinas, E. *Mater. Lett.* **1998**, *35*, 317.

(23) Ardizzone, S.; Bianchi, C. L.; Fadoni, M.; Vercelli, B. *Appl. Surf. Sci.* **1997**, *119*, 253.

(24) Gregg, S. J.; Sing, K. S. W. *Adsorption, Surface Area and Porosity*, 2nd ed.; Academic Press: London, UK, 1982.

(25) (a) Pauly, T. R.; Liu, Y.; Pinnavaia, T. J.; Billinge, S. J. L.; Bieker, T. P. *J. Am. Chem. Soc.* **1999**, *121*, 8835. (b) Wong, S. T.; Lin H. P.; Mou, C. Y. *Appl. Catal. A* **2000**, *198*, 103. (c) Zhang, L. Z.; Yu, J. C. *Chem. Commun.* **2003**, 2078.

(26) Rolison, D. R. *Science* **2003**, *299*, 1698.

(27) Fang, Y. P.; Xu, A. W.; Yu, J. C.; Wu, L.; You, L. P.; Liu, H. Q. Unpublished data.

(28) Yang, Q. B.; Li, Y. X.; Yin, Q. R.; Wang, P. L.; Cheng, Y. B. *Mater. Lett.* **2002**, *55*, 46.

(29) (a) Lu, J.; Xie, Y.; Xu, F.; Zhu, L. Y. *J. Mater. Chem.* **2002**, *12*, 2755. (b) Chen, M.; Xie, Y.; Lu, J.; Xiong, Y. J.; Zhang, S. Y.; Qian, Y. T.; Liu, X. M. *J. Mater. Chem.* **2002**, *12*, 748.

(30) (a) Mayers, B.; Xia, Y. N. *Adv. Mater.* **2002**, *14*, 279. (b) Sun, Y. G.; Gates, B.; Mayers, B.; Y. D.; Xia, Y. N. *Nano Lett.* **2002**, *2*, 165.

(31) (a) Pan, Z. W.; Dai, Z. R.; Wang, Z. L. *Science* **2001**, *291*, 1947. (b) Brenner, S. S.; Sears, G. W. *Acta Metall.* **1956**, *4*, 268. (c) Yang, P.; Lieber, C. M. *J. Mater. Res.* **1997**, *12*, 2981.